ACS APPLIED MATERIALS & INTERFACES

Research Article

www.acsami.org

Airflow-Induced Triboelectric Nanogenerator as a Self-Powered Sensor for Detecting Humidity and Airflow Rate

Hengyu Guo, Jie Chen, Li Tian, Qiang Leng, Yi Xi,* and Chenguo Hu*

Department of Applied Physics, Chongqing University, Chongqing 400044, People's Republic of China

ABSTRACT: Humidity sensors are commonly based on the resistance change of metal oxide semiconductors, which show high sensitivity in low humidity but low sensitivity in high humidity. In this work, we design a novel humidity sensor based on the airflow-induced triboelectric nanogenerator (ATNG) that can serve as a self-powered sensor to detect humidity (especially in high humidity) and airflow rate. The output current or voltage change is investigated under different humidity (20−100% relative humidity) at fixed airflow rate and different airflow rates (15−25 L/min) at a fixed humidity. The working principle of the ATNG-based sensor is illustrated. We find that both output current and voltage can serve as a variable for detecting humidity, while only the output current can serve as a variable for determining airflow rate. Our study demonstrates an innovative approach toward detection of humidity and airflow rate with advantages of self-power, multifunction, low cost, simple fabrication, and high sensitivity.

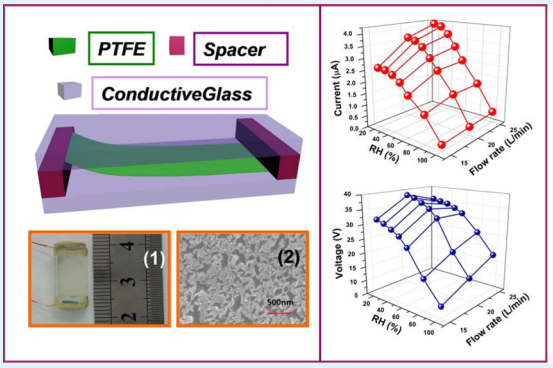

KEYWORDS: *humidity sensor, airflow rate sensor, nanogenerator, self-power, triboelectric effect, electrostatic induction*

1. INTRODUCTION

The need for humidity sensors has increased in many applications, such as air conditioning systems, food quality monitoring, and medical equipment. Therefore, humidity control is necessary for enhancing industrial processes and improving the quality of life. Nowadays, humidity sensors are mostly based on metal oxides, porous silicon, polymers, and polyelectrolytes.[1,2] However, those humidity sensors usually have high sensitivity at low humidity but go to saturation at higher humidity (>60% relative humidity, RH) with relatively long response and recovery time.[3] The sensors for measuring airflow rate are applied in the fields of biomedical engineering, environmental monitoring, and industrial process control.

A triboelectric nanogenerator (TENG) has been newly developed to convert mechanical energy into electric power for driving small electronic devices,[4] such as small liquid crystalline display (LCD) screens,[5] Li-ion batteries, capacitors,[6,7] active sensors,[4,8,9] and light emitting diodes (LEDs). As TENG can harvest energy from the ambient environment, it has been developing rapidly, and the output of TENG has been increasing greatly. In our previous work, we proposed airflow-induced triboelectric nanogenerator (ATNG) for harvesting airflow energy,[10] which was able to harvest wind energy to produce alternating electricity. Triboelectric generators have diverse applications,[4,11−13] particularly in the self-powered sensors, such as pressure sensors,[14] wind-velocity sensors,[11] transportation monitoring sensors,[15] magnetic sensors,[16] and glucose biosensors.[17] Recently, TENG acting as a self-powered active sensor to detect liquid/gaseous or water/ethanol has also been reported.[18] Because the output signals are related to the structure and driving mode,[19] the humidity sensor based on TENG should be designed in a novel structure for practical applications. It is still a challenge to explore a novel humidity sensor beyond the common resistance type to enhance its sensitivity.

Herein, we demonstrated an ATNG-based sensor for detecting humidity and airflow rate. The mechanism of the ATNG-based sensor has been illustrated. The output signals of the sensors for detecting humidity and determining air flow rate have been studied systematically. These results revealed that the sensors based on ATNG made of PTFE film have several advantages, including self-power, multifunction, low cost, simple fabrication, and high sensitivity. The self-powered sensors can be applied for environmental monitoring and industrial manufacturing.

2. EXPERIMENTAL SECTION

2.1. Fabrication of ATNG Sensor. The structure schematic diagram of the device and a digital photograph are shown in Figure 1a; the sensor is indicated with a red dashed box. An enlarged diagram and digital photograph of the sensor are shown in Figure 1b and inset 1, respectively. The fabrication process has been presented in our previous work.[10] FTO glass was chosen as electrode material due to its stability in humid conditions and because its nanostructure on the surface can somehow enhance triboelectric effect. FTO glass was cut into pieces with dimensions of 15 × 5 mm as top and bottom electrodes. In this work, we also used polytetrafluorothylene (PTFE) film (cut in dimensions of 15 × 4 mm and 50 μm in thickness) as electret material because of its wonderful capacity to hold charges and good mechanical behavior.[20,21] To enhance the charge density on the surface of PTFE, we employed the inductively coupled plasma (ICP)

Received: July 25, 2014
Accepted: September 5, 2014
Published: September 5, 2014

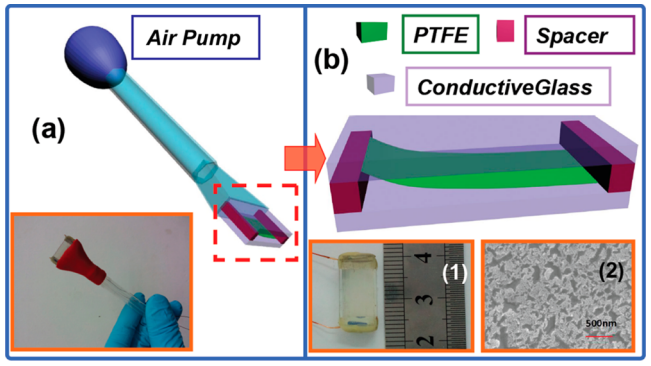

Figure 1. (a) Schematic diagram and (inset) digital photograph of the designed ATNG sensor. (b) Enlargement of the area indicated by the dashed red box in panel a, (b, inset 1) digital photograph of ATNG, and (b, inset 2) SEM image of the surface of PTFE film.

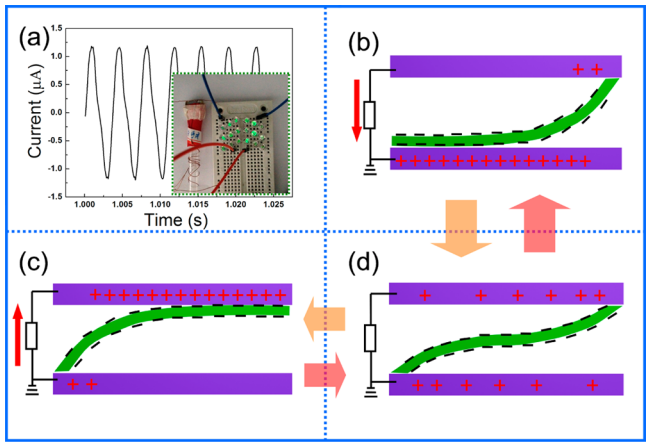

Figure 2. Mechanism diagram of ATNG-based sensor. (a) Output current curve of the sensor and (inset) digital photograph of LEDs lit by the self-powered sensor. (b–d) Processes of the working mechanism.

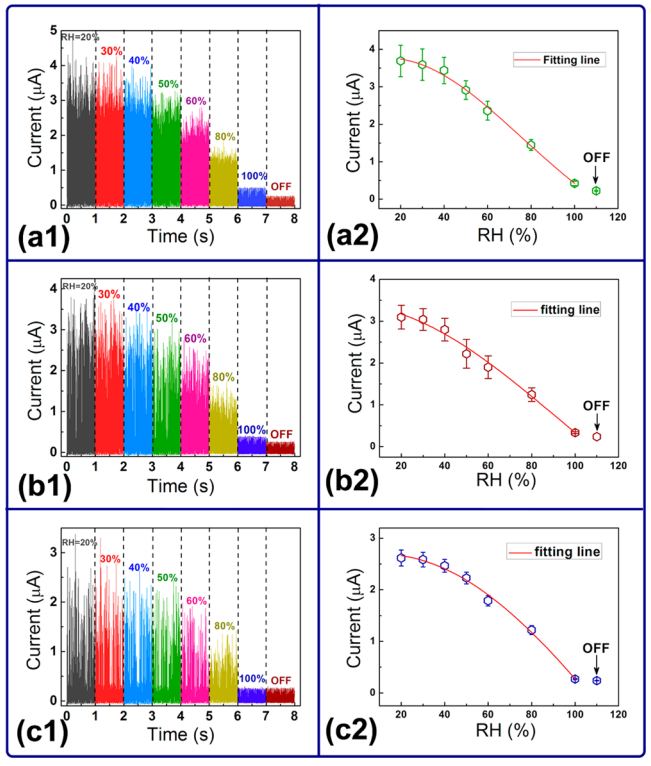

Figure 3. Output current with varying relative humidity (20–100%) under different flow rates; FR = (a1) 25, (b1) 20, and (c1) 15 L/min. (a2–c2) Corresponding spot dates of panels a1–c1.

dx.doi.org/10.1021/am504919w | ACS Appl. Mater. Interfaces 2014, 6, 17184–17189

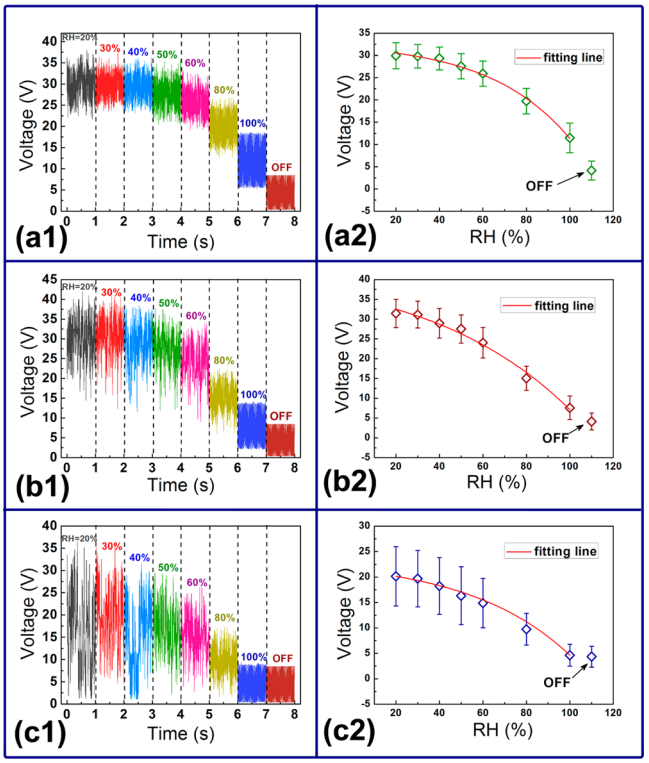

Figure 4. Output voltage (with the external load resistance of 50 MΩ) with varying relative humidity (20−100%) under different flow rates; FR = (a1) 25, (b1) 20, and (c1) 15 L/min. (a2−c2) Corresponding spot dates of panels a1−c1.

reactive ion etching to produce a surface nanostructure; typically, Ar, O_2, and CF_4 gases were introduced into the ICP chamber with flow rates of 15, 10, and 30 sccm, respectively. One power source of 400 W was used to generate a large density of plasma, while another 100 W was used to accelerate the plasma ions. The PTFE thin film was etched for 10 s in order to produce nano structures on the surface. Figure 1b, inset 2, shows an SEM image of the surface of the PTFE film, which reveals that the surface of the PTFE film is pretty rough. Later, the PTFE film was installed in the gap between two FTO glasses with conductive surface inside. Then, the assembly process was carried out by fixing the two ends of the PTFE strip onto each electrode using kapton tape with the electrode gap of 1 mm. Finally, a rubber sleeve and a PE tube (diameter, 7 mm) were used to form a structure in order to produce airflow (Figure 1a).

2.2. Characterization of the Device. The morphology of the etched PTFE surface was characterized using a field emission scanning electron microscope (Nova 400 Nano SEM). The output of the ATNG sensor was measured using a Stanford low-noise current preamplifier (Model SR570) and a Data Acquisition Card (NI PCI-6259). To obtain an experimental environment with different relative humidity, we used a benchtop transparent glovebox (EQ-VGB-2, MTI, China), an air humidifier (GO-2080, GOAL, China), a hygrometer (HG135, HG, China), and several desiccants to produce and control various humidity conditions. During the test, we used a small mechanical pump to generate airflow which concatenates a rotameter to determine the flow rate.

3. RESULTS AND DISCUSSION

3.1. Working Principle of the TENG. Figure 2a and the inset show the working state of the ATNG, indicating that the output short current of 1.25 μA can light 18 LEDs. Figure 2b−d presents the side view of the ATNG, which is considered to be a flat-panel capacitor with an external load of R. The working principle of the TENG depends on the combination of triboelectrification and electrostatic induction. The induced charge density (σ_b) on the bottom electrode (under short current) is

$$\sigma_b = -\left(\frac{d - d_1}{d}\right)\sigma$$

The PTFE film vibrates with air flowing through the ATNG, and the PTFE film is charged by rubbing against the two electrodes, resulting in a negative charge on the two surfaces of the PTFE film and a positive charge on the two electrodes. After the triboelectric action process, the PTFE film is charged with a constant charge density ($\sigma < 0$). When the film approaches the top electrode, electrons from the top electrode would transfer to the bottom electrode through the external circuit because of the rejection of the charges. When the film carried with negative charges approaches the bottom electrode, electrons from the bottom electrode were also transferred to the top electrode. Because σ is a constant, the induced charge density on the bottom electrode ($\sigma_b > 0$) varies with the position of the PTFE film between the two electrodes. However, as the σ on the PTFE film is very sensitive to humidity, the output signal can be used to detect humidity, and as the PTFE film vibration frequency is related to airflow rate, the output signal can also be used to detect flow rate.

3.2. ATNG Sensor for Detecting Humidity. The output short current of the ATNG sensor is carefully studied by a single variable control method. In order to demonstrate that the device can be a self-powered sensor for detecting ambient environment humidity, we measured the performance of the ATNG sensor in a glovebox with different relative humidity (RH) under the same flow rate (FR) conditions. Various RH values include 0, 20, 40, 60, 80, and 100%. The output short current after rectification is shown in Figure 3a1−c1. These results indicate that the output short current decreases as the

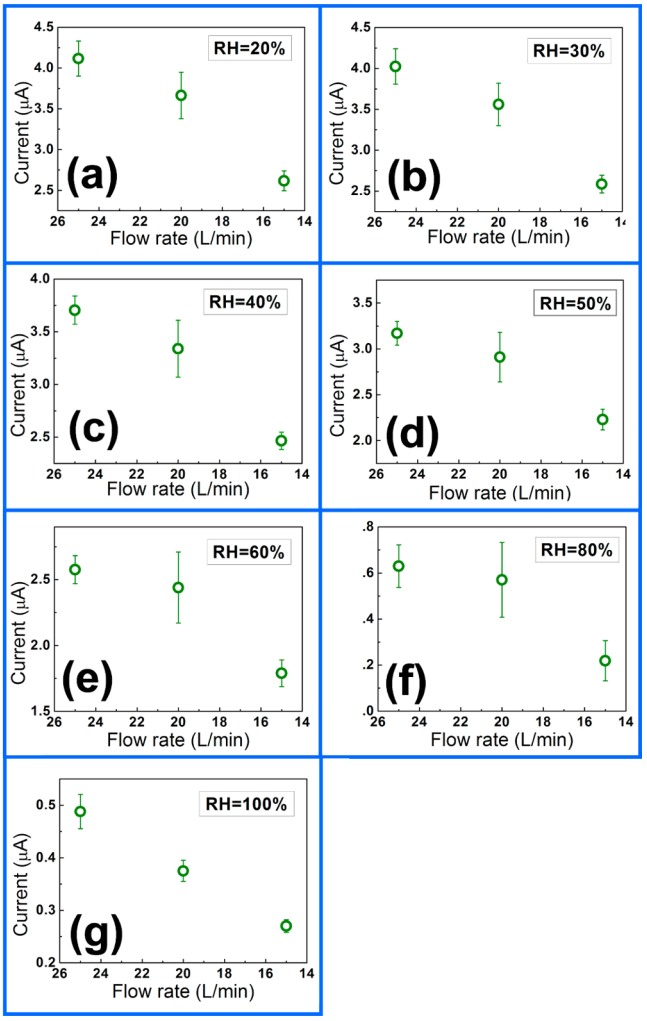

Figure 5. Relationship between output current and flow rate under varying relative humidity; RH = (a) 20, (b) 30, (c) 40, (d) 50, (e) 60, (f) 80, and (g) 100%.

RH increases. The plot of the short current versus RH is drawn in Figure 3a2−c2, and the fitting line indicates that with the increase in RH from 20 to 100%, the output signals decrease from ∼4.1 to ∼0.5 μA at FR = 25 L/min (Figure 3a2), from ∼3.7 to ∼0.3 μA at FR = 20 L/min (Figure 3b2), and from ∼2.6 to ∼0.2 μA (background current) at FR = 15 L/min (Figure 3c2). The above experimental results suggest that output current can be used as detection variable when the external environment FR is a certain value and the higher sensitivity can be obtained at higher flow rate.

The output voltage of the ATNG sensor is also measured under different RH with an external load resistance of 50 MΩ, as are shown in Figure 4a1, b1 and c1, indicating the output voltage decreases with a RH increase. The plot of the output voltage versus RH is drawn in Figure 4a2−c2. With RH increasing from 20% to 100% the rectification of output voltage drops from ∼36 to ∼18 V at FR = 25 L/min (4a2), from ∼38 to ∼13 V at FR = 20 L/min (4b2), and from ∼32 to ∼9 V at FR = 15 L/min (4c2). The results demonstrate that the output voltage can also be used as variable to detect the humidity and the higher airflow rate can provide higher stability of the sensor.

3.3. ATNG Sensor for Detecting Airflow Rate. To investigate the ATNG sensor as a self-powered device for detecting FR, we make sure that RH is constant when FR varies from 15 to 25 L/min. The measurement results are shown in Figure 5, from which we can see that faster FR results in a higher output current, and lower RH gives higher short current. The biggest short current of 4.2 μA is achieved at 20% RH. The fitting line indicates the output signals nonlinearly decrease with a decrease in FR, except for the output current of the sensor when RH is 100%, which could not be trusted due to the signal closing to background. The above experimental results indicate that when the external environment RH is less than 80%, output current can be used as detection variable for FR.

Figure 6 exhibits the output voltage of the sensor under different FR ranging from 15 to 25 L/min for a given external load resistance (50 MΩ), revealing an irregular change trend with the decrease in FR, except for the output voltage of the sensor when RH comes to 80 and 100%. From the previous report, we know that the vibration frequency increases with an increase in airflow rate, but a vibration frequency that is too fast can reduce the effective contact area, which results in a smaller output voltage.[10] Therefore, the fitting line rises with a decrease in FR at the beginning, instead of a direct drop. But when the RH reach a certain value (>80%), the PTFE film adsorbs many of the water molecules that shield the charges on the film and leads to a clear drop trend with a decrease in FR, as are shown in Figure 6f,g. Because RH is not a monotone decreasing with

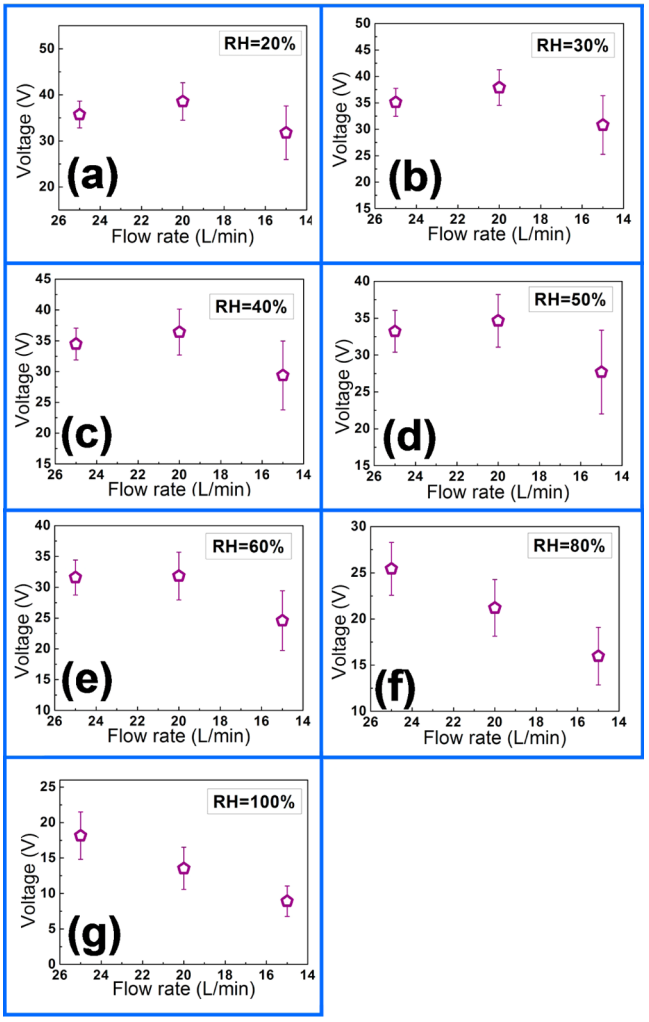

Figure 6. Relationship between output voltage (external load resistance of 50 MΩ) and flow rate under varying relative humidity; RH = (a) 20, (b) 30, (c) 40, (d) 50, (e) 60, (f) 80, and (g) 100%.

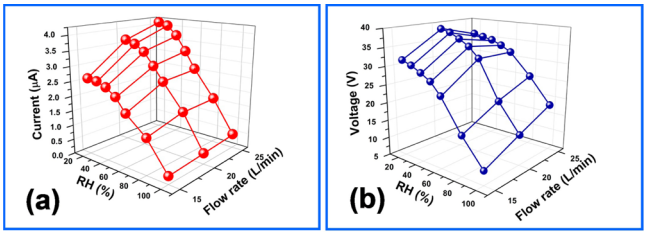

Figure 7. Three-dimensional graphs of ATNG sensor response to the changing external RH and FR. (a) Short current response. (b) Voltage (external load resistance of 50 MΩ) response.

the output voltage, the output voltage can not be used as a detection variable for detecting FR in RH ≤ 60%.

The ATNG-based sensor response to the changing RH and FR are systematically investigated, and the results are extracted and plotted in a three-dimensional (3D) graph. The overall change trend of the output short current with change in RH and FR can be simultaneously derived from Figure 7a. Obviously, the output signal decreases with an increase in RH, while an opposite change occurs with the variation in FR. Figure 7b presents the output voltage changes with variation in RH and FR for a given external load resistance (50 MΩ). The output voltage signal decreases with an increase in RH and increases as the FR goes up.

4. CONCLUSIONS

In summary, the ATNG based on the airflow-induced vibration of a PTFE film between two electrodes has been designed and used as self-powered sensors for detecting humidity and airflow rate without an external power source. The working principle of the ATNG sensor has been illustrated. As for a self-powered humidity sensor, the output voltage and short current can be used as detection variables. However, as a self-powered airflow rate sensor, only the output short current can serve as a detection variable because the output voltage is not in monotone change with respect to flow rate. Our study suggests that these ATNG devices can be applied as self-powered sensors for environmental monitoring and industrial manufacturing with

advantages of self-power, multifunction, low cost, simple fabrication, and high sensitivity.

AUTHOR INFORMATION

Corresponding Authors

*Tel: +86 23 65678362. Fax: +86 23 65678362. E-mail: hucg@cqu.edu.cn.

*E-mail: yxi6@cqu.edu.cn.

Notes

The authors declare no competing financial interest.

ACKNOWLEDGMENTS

This work is supported by the NSFCQ (cstc2012jjB0006), SRFDP (20110191110034, 20120191120039), NSFC (11204388), and the Fundamental Research Funds for the Central Universities (CDJRC10300001, CDJZR11300004, CDJZR12225501, and CQDXWL-2013-012).

REFERENCES

(1) Chen, Z.; Lu, C. Humidity Sensors: A Review. *Sens. Lett.* **2005**, *3*, 274−295.

(2) Lee, C. Y.; Lee, G. B. Humidity Sensors: A Review of Materials and Mechanisms. *Sens. Lett.* **2005**, *3*, 1−15.

(3) Zhang, M. C.; Hu, C. G.; Liu, H.; Xiong, Y. F.; Zhang, Z. W. A Rapid-Response Humidity Sensor based on $BaNbO_3$ Nanocrystals. *Sens. Actuators, B* **2009**, *136*, 128−132.

(4) Fan, F. R.; Tian, Z. Q.; Wang, Z. L. Flexible Triboelectric Generator. *Nano Energy* **2012**, *1*, 328−334.

(5) Hu, Y. F.; Zhang, Y.; Xu, C.; Zhu, G.; Wang, Z. L. High-Output Nanogenerator by Rational Unipolar Assembly of Conical Nanowires and its Application for Driving a Small Liquid Crystal Display. *Nano Lett.* **2010**, *10*, 5025.

(6) Wang, S. H.; Lin, L.; Wang, Z. L. Nanoscale Triboelectric-Effect-Enabled Energy Conversion for Sustainably Powering Portable Electronics. *Nano Lett.* **2012**, *12*, 6339−6346.

(7) Zhong, Q. Z.; Zhong, J. W.; Hu, B.; Hu, Q. Y.; Zhou, J.; Wang, Z. L. A Paper-Based Nanogenerator as a Power Source and Active Sensor. *Energy Environ. Sci.* **2013**, *6*, 513−518.

(8) Yang, W. Q.; Chen, J.; Wen, X. N.; Jing, Q. S.; Yang, J.; Wang, Z. L. Triboelectrification-based Motion Sensor for Human-Machine Interfacing. *ACS Appl. Mater. Interfaces* **2014**, *6*, 7479−7484.

(9) Yang, Y.; Zhang, H. L.; Zhong, X. D.; Yi, F.; Yu, R. M.; Wang, Z. L. Electret Film-Enhanced Triboelectric Nanogenerator Matrix for Self-Powered Instantaneous Tactile Imaging. *ACS Appl. Mater. Interfaces* **2014**, *6*, 3680−3688.

(10) Guo, H. Y.; He, X. M.; Zhong, J. W.; Zhong, Q. Z.; Hu, C. G.; Zhou, J. A Nanogenerator for Harvesting Airflow Energy and Light Energy. *J. Mater. Chem. A* **2014**, *2*, 2079.

(11) Zhang, R.; Lin, L.; Jing, Q. S.; Wu, W. Z.; Zhang, Y.; Jiao, Z. X.; Wang, Z. L. Nanogenerator as an Active Sensor for Vortex Capture and Ambient Wind-Velocity Detection. *Energy Environ. Sci.* **2012**, *5*, 8528−8533.

(12) Sun, C. L.; Shi, J.; Bayerl, D. J.; Wang, X. D. PVDF Microbelts for Harvesting Energy from Respiration. *Energy Environ. Sci.* **2011**, *4*, 4508−4512.

(13) Yang, Y.; Zhu, G.; Zhang, H. L.; Chen, J.; Zhong, X. D.; Wang, Z. L. Triboelectric Nanogenerator for Harvesting Wind Energy and as Self-Powered Wind Vector Sensor System. *ACS Nano* **2013**, *7*, 9461−9468.

(14) Fan, F. R.; Lin, L.; Zhu, G.; Wu, W. Z.; Zhang, R.; Wang, Z. L. Transparent Triboelectric Nanogenerator and Self-Powered Pressure Sensor based on Micropatterned Plastic Films. *Nano Lett.* **2012**, *12*, 3109−3114.

(15) Lin, L.; Hu, Y. F.; Xu, C.; Zhang, Y.; Zhang, R.; Wen, X. N.; Wang, Z. L. Transparent Flexible Nanogenerator as Self-Powered Sensor for Transportation Monitoring. *Nano Energy* **2013**, *2*, 75−81.

(16) Yang, Y.; Lin, L.; Zhang, Y.; Jing, Q. S.; Hou, T. C.; Wang, Z. L. Self-Powered Magnetic Sensor based on a Triboelectric Nanogenerator. *ACS Nano* **2012**, *11*, 10378−10383.

(17) Zhang, H. L.; Yang, Y.; Hou, T. C.; Su, Y. J.; Hu, C. G.; Wang, Z. L. Triboelectric Nanogenerator Built Inside Clothes for Self-Powered Glucose Biosensors. *Nano Energy* **2013**, *2*, 1019−1024.

(18) Zhang, H. L.; Yang, Y.; Su, Y. J.; Chen, J.; Hu, C. G.; Wu, Z. K.; Liu, Y.; Wong, C. P.; Bando, Y. S.; Wang, Z. L. Triboelectric Nanogenerator as Self-Powered Active Sensor for Detecting Liquid/Gaseous Water/Ethanol. *Nano Energy* **2013**, *2*, 693−701.

(19) Zhong, J. W.; Zhong, Q. Z.; Fan, F.; Zhang, Y.; Wang, S.; Hu, B.; Wang, Z. L.; Zhou, J. Finger Typing Driven Triboelectric Nanogenerator and its Use for Instantaneously Lighting up LEDs. *Nano Energy* **2013**, *2*, 491−497.

(20) Baland, J.; Chao, Y. H.; Suzuki, Y.; Tai, Y. C. Micro Electret Power Generator. In *Proceedings of the 16th IEEE International Conference on Micro Electro Mechanical Systems*, Kyoto, Japan, Jan. 23, 2003; p 538.

(21) Malecki, J. A. Linear Decay of Charge in Electrets. *Phys. Rev. B: Condens. Matter Mater. Phys.* **1999**, *59*, 9954.